applied sciences

MDPI

Article

The Contact Phase in Vehicle–Pedestrian Accident Reconstruction

Bogdan Benea and Adrian Soica *

Department of Automotive and Transport Engineering, Transilvania University of Brasov, 500036 Brasov, Romania; b.benea@unitbv.ro
* Correspondence: a.soica@unitbv.ro

Abstract: The need for continuous research to refine the models used in forensic accident reconstruction appears with the development of new car models that satisfy consumer complaints. This paper analyzed a sub-sequence of car and pedestrian accidents from the perspective of the distance traveled by them in the contact phase with the aim of improving the information regarding the reconstruction of road accidents. This research included the analysis of some real tests with pedestrian dummies, as well as simulations of the impact between different classes of vehicles and pedestrians in two different walking positions. Specialized software was used with complex multibody models of pedestrians, modifying the speed and deceleration parameters of the car at the time of the collision. For pedestrian characteristics, the friction coefficients of the ground, car and its mass were modified. The research results highlight the differences between the bilinear models used in accident reconstruction and the proposed study. They can also be used to determine the distance traveled by the vehicle in the first phase of a collision with pedestrians.

Keywords: vehicle–pedestrian collision; accident reconstruction; contact phase; contact distance

Citation: Benea, B.; Soica, A. The Contact Phase in Vehicle–Pedestrian Accident Reconstruction. *Appl. Sci.* **2023**, *13*, 9404. https://doi.org/10.3390/app13169404

Academic Editor: Yosoon Choi

Received: 8 July 2023
Revised: 30 July 2023
Accepted: 4 August 2023
Published: 18 August 2023

1. Introduction

Traffic accidents in which vulnerable participants such as cyclists and pedestrians are involved have been studied over time, first with the aim of reconstructing the events, followed by the establishment of empirical or mathematical models which take into account a series of factors regarding the throwing distance of pedestrians. In the specialized literature, extensive studies have been published by many authors, starting from the 1970s. An objective of these analyses consists in determining the throw distance of the pedestrian. In [1–5], various formulas for determining these distances were proposed depending on various factors, such as the impact speed, the angle of throw from the hood, the height of the center of mass of the pedestrian, the coefficient of friction between the pedestrian and the ground, the mass of the vehicle and the pedestrian, and the deceleration of the vehicle at the time of impact.

In [6,7], three phases of vehicle–pedestrian impact were identified by Eubanks, Hait and Limpert. These are the contact phase, the flight phase (throwing through the air) and the rolling/sliding phase on the ground. According to pedestrian dynamics, five categories of vehicle−pedestrian collisions are described in [8,9]. These are wrap, forward projection, fender vault, roof vault and somersault collisions [10]. The contact phase, with the duration of the interval between the first impact and the secondary contact, was studied in 2001 by Han and Brach, who proposed the bilinear model regarding the distance traveled by the vehicle and the pedestrian in this stage. This model takes into account the position of the center of mass in relation to the vehicle.

In [11], it is considered that this phase lasts approximately 0.2 s, during which it is approximated that the pedestrian travels a distance of 2 m without specifying exactly which element of the body detaches last from the vehicle. In [12], the authors break down the contact phase into two sub-phases, as shown in Figure 1. The first lasts from the initial impact until the pedestrian hits his head/chest against the windshield/hood (secondary

impact); the second extends over the period that the pedestrian remains in contact with the car after the secondary impact until separation from the vehicle. The model takes into account the last element of the body that detaches from the vehicle, excluding the upper limbs of the pedestrian from the contact analysis.

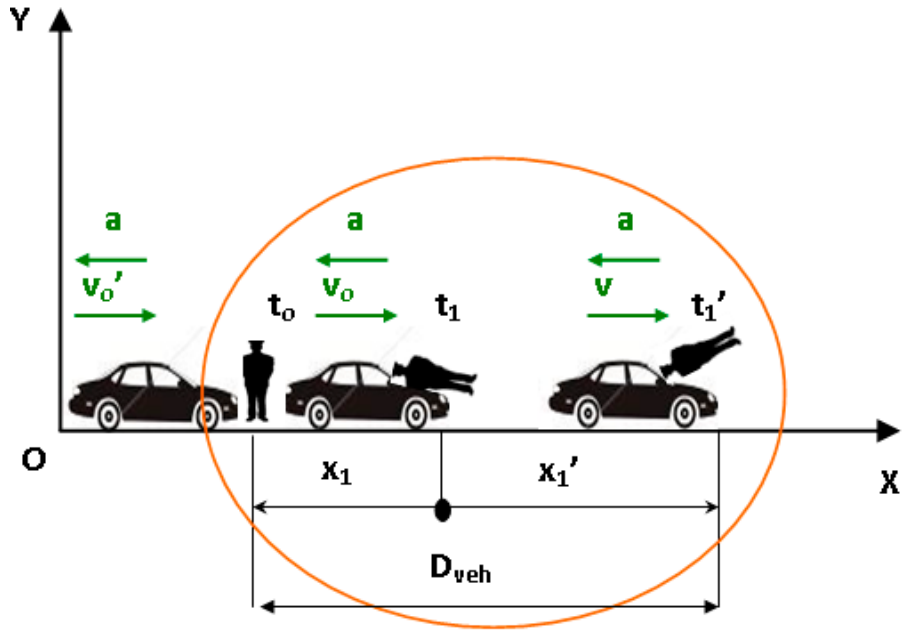

Figure 1. Vehicle–pedestrian contact phase schema.

This phase of contact distance influences others; a simple model is presented in Figure 1. It is assumed that the impact between a vehicle and a pedestrian is plastic. In this case, from the conservation of momentum law, the distance that the pedestrian is in contact with vehicle was successively determined in [12].

$$x_1 = \frac{\left(\frac{v_o'}{1+\frac{m_p}{m_v}} + a \cdot t_1\right)^2 - \left(\frac{v_o'}{1+\frac{m_p}{m_v}}\right)^2}{2 \cdot a} \quad (1)$$

$$x_1' = -\frac{\left[\left(\frac{v_o'}{1+\frac{m_p}{m_v}}\right) + a \cdot t_1\right]^2 \cdot (\eta^2 - 1)}{2 \cdot a} \quad (2)$$

$$D_{veh} = x_1 + x_1' \quad (3)$$

According to [12], the distances travelled by the vehicle and pedestrian in the contact phase are given in Relations (1)–(3), where:

v_o': vehicle speed at the moment of the first contact with the pedestrian, m/s;
v_o: speed of the vehicle–pedestrian assembly immediately after the first contact, m/s;
v: vehicle speed at the moment of secondary impact, m/s;
a: average brake deceleration from the moment prior to the first impact with the pedestrian, m/s^2;
m_v: vehicle mass, kg;
m_p: pedestrian mass, kg;
t_0: time at which the pedestrian is hit by the vehicle, s;
t_1: time at which the pedestrian hits the hood–windshield area with the head, s;
t_1': time at which the pedestrian is detached from the vehicle, s;
x_1: the space covered by the vehicle–pedestrian assembly in sub-phase 1.1, m;
x_1': the space covered by the vehicle–pedestrian assembly in sub-phase 1.2, m;

D_{veh}: the space covered by the pedestrian in the contact phase with the vehicle, phase 1, m;

η: pedestrian impact factor.

In [13], the authors also show the existence of two sub-phases in the vehicle contact phase. In Figure 2, a sample sequence of pedestrian kinematics at different timings and phases during the vehicle impact process is demonstrated: "t_0" is the first vehicle–pedestrian contact time and "t_1" is the first vehicle–head impact time. Then, the pedestrian moves together with the car until "t_2", when they separate.

Figure 2. Vehicle–pedestrian impact.

2. Research Motivation

The specialized literature addressing vehicle–pedestrian accidents illustrates various models/formulas that divide the stages of the collision into three phases, i.e., contact with the vehicle, flying through the air and rolling on the ground, with the aim of establishing the total distance of pedestrian throw. The first phase was succinctly analyzed in [12–14], where two sub-phases were highlighted.

Analyses of real collisions between vehicles and dummies, as well as modeling with especially dedicated software [15–17], were carried out for the study of the contact phase between a vehicle and a pedestrian. This should allow specialists to more accurately investigate the circumstances of pedestrian accidents.

In this paper, we intend to improve the proposed bilinear model by establishing a relation regarding the distance traveled by the pedestrian during the contact phase with the vehicle depending on the collision speed. Some of the factors that influence pedestrian kinematics will be analyzed, such as the typology of the body shape, vehicle deceleration, pedestrian mass and friction coefficient with the car and the ground, using car models frequently encountered on roads nowadays.

3. Research Methods and Models

This research was conducted by simulating a vehicle–pedestrian collision on a dry asphalt surface on a horizontal road section, which is the preponderant scenario. Impact conditions in rainy weather were also simulated in order to observe the influence on the change in the traveled distance. Thus, the coefficients of friction between the pedestrian and the vehicle, respectively, and the ground were reduced.

Therefore, the research results of this stage can only be applied to traffic accidents that occur in these conditions.

As shown in [18–20], rain decreases the number of vehicle–pedestrian accidents. Some of the possible factors that led to these research results are as follows:

- Cars slow down due to drivers who are not accustomed to driving in wet conditions;
- Mixed effects affecting both crash risk and exposure;
- Poor weather conditions reduce accidents by discouraging driving and leading to fewer drivers and less congested roads.

We analyzed real accidents with pedestrian dummies with images captured with high-speed cameras and simulations performed in PC-Crash.

PC-CRASH, multibody solvers, utilizes a contact algorithm similar to MADYMO, i.e., an algorithm based on the calculation of the depth of penetration [21].

To validate the proposed model, a nine cases were extracted from the experimental tests and were submitted to simulations that were carried out under the same conditions in PC-Crash. The obtained results indicate a maximum difference of −10% and +12% between analyses. During the experimental tests, the resistance structure of the dummy failed in two situations, with values of over 4 m being subsequently recorded. In another situation, at low impact speed, the dummy was hit from behind, not from the side, thus resulting in a long transport distance, the pedestrian being carried on the hood and then sliding in front of the vehicle, as indicated in Figure 3.

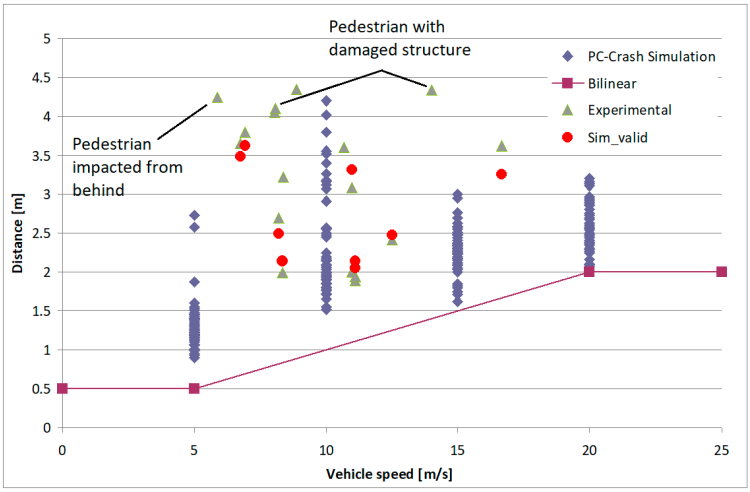

Figure 3. Validation results of the vehicle–pedestrian impact.

The multibody pedestrian body elements (head, torso, pelvis, etc.) are interconnected with pivoting joints. For each body, there are different properties such as geometry, mass, contact stiffness and coefficients of friction. A general ellipsoid of degree "n" specifies the geometry for each body. The pedestrian and occupant multibodies are modeled with 20 bodies interconnected by 19 joints [22].

For each body of the multibody system, the following properties can be specified independently:

- Body geometry is represented by ellipsoid shapes; the length along each axis and the degree of the ellipsoid can be specified;
- The moments of inertia of each body and its mass;
- Stiffness coefficient for each body used when calculating contact forces;
- Coefficients of friction can also be specified. One is used for ellipsoid-to-vehicle contacts; the other is used for ellipsoid-to-ellipsoid and ellipsoid-to-ground contacts.

On account of the fact that the geometry of the vehicle can have a significant effect on the pedestrian dynamics, the model enables the use of different vehicle shapes. In Figure 4 and Table 1, we present the main data of the vehicles used in simulation. The vehicle shape can be either specified using the menu item, or a detailed 3D DXF shape can be imported and attached to the vehicle [22]. The model uses a linear stiffness model with restitution [23].

In PC-Crash, the simple 3D DXF vehicle shape is used for the calculation. Each vehicle folder contains 2 DXF models, one with the same name as the vehicle model, a second with the name "output.dxf". The second is better for contact calculations with multibody systems because the mesh is more simplified and uniform.

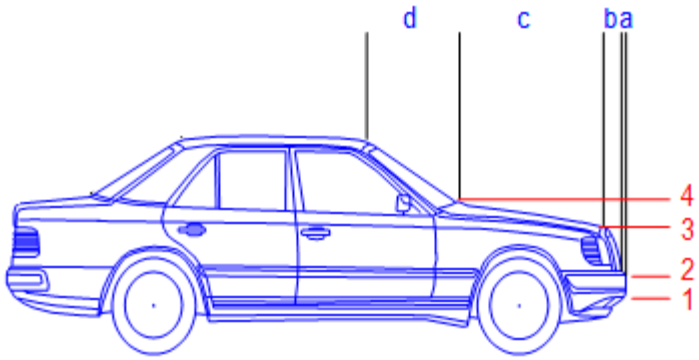

Figure 4. Vehicle geometrical characteristics, source [22].

Table 1. Vehicle characteristics; source: PC-CRASH.

Vehicle Type	Mass [kg]	Height [m]	a [m]	b [m]	c [m]	d [m]	1 [m]	2 [m]	3 [m]	4 [m]
SM-1	795	1.465	0.050	0.058	0.871	0.498	0.350	0.500	0.837	0.942
SM2	854	1.489	0.050	0.052	0.904	0.517	0.350	0.500	0.851	0.957
CC-1	1390	1.410	0.050	0.065	1.142	0.653	0.350	0.500	0.806	0.906
CC-2	1180	1.420	0.050	0.064	1.124	0.642	0.350	0.500	0.811	0.913
CC-3	1395	1.462	0.050	0.067	1.167	0.667	0.350	0.500	0.835	0.940
CC-4	1025	1.535	0.050	0.063	1.096	0.626	0.350	0.500	0.877	0.987
CSUV-1	1585	1.700	0.050	0.065	1.130	0.646	0.350	0.500	0.971	1.093
CSUV-2	1280	1.630	0.050	0.063	1.102	0.630	0.350	0.500	0.931	1.048
EC-1	2135	1.480	0.050	0.076	1.335	0.763	0.350	0.500	0.846	0.951

Additionally, users can input custom dimensions. The vehicle shape specified here is used to determine the vehicle ellipsoid sizes for the stiffness-based impact/rollover model. The shape is also used for collisions with multibody objects, unless a DXF/IDF vehicle shape is specified for these contacts. Custom vehicle multibodies can be specified for interaction with other multibodies [22]. Properties for stiffness-based impacts can be also specified as follows:

- Friction—This is the coefficient of friction for the vehicle body.
- Restitution—This is the coefficient of restitution for vehicle impacts. If the stiffness-based impact model is used, only one restitution coefficient for all concerned vehicles should be used.
- Stiffness—This is expressed as a deformation distance. For passenger cars, the specified stiffness is for the lower part of the vehicle body only. For the roof, one quarter of the specified stiffness is used.

Multibody forensic models available in reconstruction software were often validated by comparing body motion with video data either from dummy crash tests or CCTV recordings [21]. In [24,25], the authors used camera images from real accidents involving pedestrians as a technique for accident analysis.

The videos were recorded over time, with different high-speed cameras at the rate of 500 or 1000 fps, with image resolution of 845 × 480 and 640 × 480 pixels. The position of the cameras was fixed; the filming was carried out in open spaces with strong sunlight or in laboratory with special lighting facilities. The collision speed and the vehicles deceleration were determined with datalogger-type measuring equipment that includes accelerometers. To establish the travel distance, we used photogrammetric techniques, with at least one known dimension.

The simulations analyzed pedestrians in a walking posture, crossing in front of a vehicle, perpendicular to their direction of travel. These types of accidents were also revealed in [26]. The authors showed that when focusing on the distribution ratio of the cases when pedestrians were crossing the roads in front of the forward moving cars, these were 67% (fatal) in daytime and 78% at night-time. Two different cases of first contact in the leg area were analyzed, namely when the body weight is taken on the front leg (P1) and when it is taken on the rear leg during walking (P2), as shown in Figure 5.

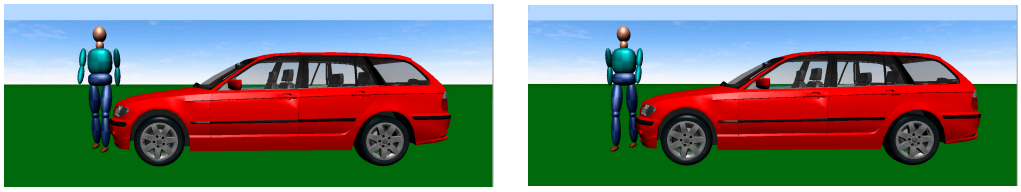

Figure 5. Pedestrian positions at the time of the impact.

The simulation was carried out in 3D. During the simulation, collisions occurred between the car and the pedestrian at different vehicle speeds.

These were modeled by accepting the following initial data:

- The types of vehicles involved in the collision were the following: compact class-CC, super-mini class-SMC, executive class-EC and compact SUV-CSUV;
- Vehicle initial speed was 5, 10, 15 and 20 m/s;
- Vehicle deceleration during impact was 0, 2.5, 5 and 7.5 m/s^2;
- Pedestrian walking perpendicular to vehicle direction at 1.4 m/s;
- The coefficient of friction between vehicle and pedestrian is 0.2;
- The moment when the contact force between the body segment (head/torso) and the vehicle is zero is considered to be the moment of separation from the vehicle, as illustrated in Figure 6.

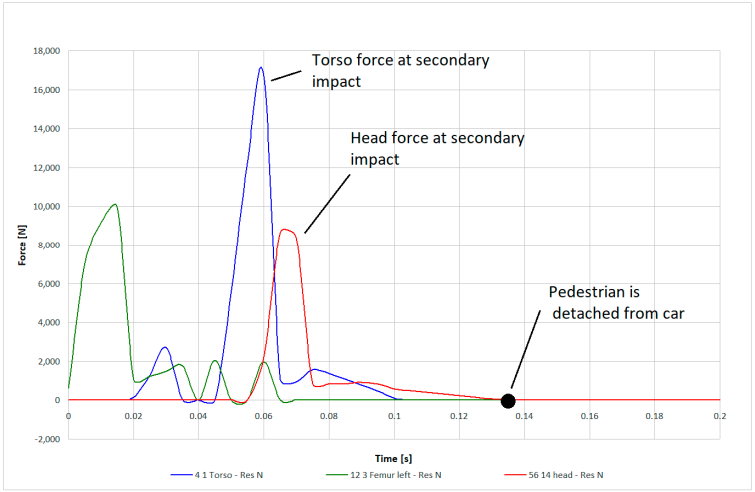

Figure 6. Example of pedestrian contact forces during impact with car.

Various areas of the body come into contact with the vehicle during the impact, but only the lower limbs, chest and head were considered in our analyses.

In [27], various body postures were defined while walking based on previous studies that state that the pedestrian's posture at the moment of impact influences the kinematics of the impact between the car and the pedestrian. Using MADYMO model, Crocetta et al. [28] selected six initial stance configurations from the gait cycle defined in [20]. In the simulations performed by the authors, impacts were performed with the pedestrian moving transversally (walking) to the vehicle at a speed of 1.4 m/s. A summary of the simulations performed is given in Table 1.

Shang et al. [29] used MADYMO ellipsoid multibody pedestrian model and real test with cadavers, performed over a speed range of 20–30 kph and with three different vehicle types and pedestrian sizes, and found a good capacity to predict vehicle contact times.

In [30], the MADYMO ellipsoid multibody pedestrian model is also used. Each model consists of 52 rigid bodies with an outer surface described by 64 ellipsoids. The MADYMO models were used to study accident reconstructions, particularly those involving vulnerable road users [31–33].

Stevenson [34] carried out an extensive study on the friction coefficients that occur in traffic accidents involving pedestrians. A non-linear frictional contact model in vehicle–pedestrian accidents was considered in [35]. The study based on their model indicates that the pedestrian–ground friction coefficient is not consistent. The relationship between the friction force and the contact pressure is non-linear.

In [36], the authors chose to use in their research the friction coefficients between the pedestrian and the ground with a value of 0.6, and between the pedestrian and the vehicle with a value of 0.3.

The dummy used had the characteristics shown in Table 2 during simulations. The moments in the main joints of the body (torso, neck, knees, and ankles) were adapted to mimic the human body as closely as possible. Studies of moments in various body joints in different postures were carried out for the knee [37], for the walking posture [38], including the hip, knees and ankles, and for the neck [39].

Table 2. Pedestrian default characteristics data.

Pedestrian male adult	Age Mass	18 years 75 kg
	Height No of body elements Friction coefficient with car	1.75 m 20 0.20
	Friction coefficient with ground	0.60

Body data are adjusted according to the report "International Data on Anthropometry" by Hans W. Jurgens, Ivar A. Aune and Ursula Pieper, published by the Federal Institute for Occupational Safety and Health, Dortmund, Federal Republic of Germany and a study made by various scientists in Slovakia [22], as shown in Table 2.

A summary of the performed simulations is given in Table 3.

Table 3. Simulation diagram.

Nr crt	Vehicle Type	No of Vehicles Studied	Vehicle Initial Speed	Vehicle Deceleration	Pedestrian Type	Pedestrian Stance	Pedestrian Initial Speed
1	CC	4	5	0, 2.5, 5, 7.5	MBD	P1, P2	1.4
		4	10	0, 2.5, 5, 7.5	MBD	P1, P2	1.4
		4	15	0, 2.5, 5, 7.5	MBD	P1, P2	1.4
		4	20	0, 2.5, 5, 7.5	MBD	P1, P2	1.4
2	SMC	2	5	0, 2.5, 5, 7.5	MBD	P1, P2	1.4
		2	10	0, 2.5, 5, 7.5	MBD	P1, P2	1.4
		2	15	0, 2.5, 5, 7.5	MBD	P1, P2	1.4
		2	20	0, 2.5, 5, 7.5	MBD	P1, P2	1.4
3	CSUV	2	5	0, 2.5, 5, 7.5	MBD	P1, P2	1.4
		2	10	0, 2.5, 5, 7.5	MBD	P1, P2	1.4
		2	15	0, 2.5, 5, 7.5	MBD	P1, P2	1.4
		2	20	0, 2.5, 5, 7.5	MBD	P1, P2	1.4

Table 3. *Cont.*

Nr crt	Vehicle Type	No of Vehicles Studied	Vehicle Initial Speed	Vehicle Deceleration	Pedestrian Type	Pedestrian Stance	Pedestrian Initial Speed
4	EC	2	5	0, 2.5, 5, 7.5	MBD	P1, P2	1.4
		2	10	0, 2.5, 5, 7.5	MBD	P1, P2	1.4
		2	15	0, 2.5, 5, 7.5	MBD	P1, P2	1.4
		2	20	0, 2.5, 5, 7.5	MBD	P1, P2	1.4

4. Results

The simulations show the existence of the two sub-phases of the contact between the vehicle and the pedestrian for all the cases analyzed, as indicated in Figure 5. With the exception of low collision speeds, the resulting types of impact are roof vault and somersault. The increase in speed at the moment of impact results in a larger movement of the pedestrian as he/she detaches from the car, performing somersaults through the air.

For an impact speed of 5 m/s, the type of impact is wrapped around; the pedestrian is not thrown through the air but slides off the vehicle.

The time when the pedestrian detaches from the vehicle is obtained from the diagram of the contact forces between the body segments and the car.

For the compact class CC vehicle, as indicated in Figure 7, the maximum distance in this case is around 4.01 m at a speed of 10 m/s, as shown in Figure 8. At the same time, we observe that the greatest variation in the distances travelled during the contact phase depends on the impact speed. The minimum distance is 1.2 m at a collision speed of 5 m/s. For this category of cars, at low impact speeds, the pedestrian kinematics is wrap around, according to the classification in [8], followed by the somersault and roof vault at high speed.

Depending on the position of the pedestrian (left leg in front or behind), as well as the offset of the impact position from the center of the car, at low speeds, we could have a fender vault collision.

Considering the time origin at the moment of impact between the bumper and the pedestrian's foot, the secondary collision occurs within a time range of 0.075 s to 0.21 s, and the detachment from the car within a time range of 0.125 s to 0.515 s, depending on speed and deceleration.

The impact moments captured in Figure 7 show the first contact in the knee region of the lower limbs, followed by the contact of the femur with the front edge of the hood. The pedestrian then strikes the hood with the thorax while the secondary, head impact occurs in the hood–windscreen area. Until detached from the vehicle, the pedestrian undergoes a roof vault or somersault movement for high speed collisions.

The low height geometric profile of some vehicles in this class leads to a high number of roof vault impacts compared to SUVs.

For the CSUV class, the maximum distance in this case is just over 2.6 m at 20 m/s, as displayed in Figure 9. In this case, there is less dispersion, as a function of impact speed, of the distances travelled during the contact phase. The minimum distance is 0.8 m at a collision speed of 5 m/s, which is the smallest in all the vehicle classes analyzed. For this class of cars, at low impact speeds, the pedestrian kinematics is wrap around, followed by the somersault and roof vault at high speed.

Considering the time origin at the moment of impact between the bumper and the pedestrian's lower limb, the secondary collision occurs within the time range of 0.06 s to 0.18 s, and the detachment from the car within the time range of 0.115 s to 0.30 s.

The impact moments captured in Figure 10 show the first contact in the knee region of the lower limbs, followed by contact of the pelvis with the front edge of the hood. The pedestrian then strikes the hood with the thorax, while the secondary head impact occurs

in the hood area at high speed. At collision speeds of 5 m/s, for this type of vehicle, it is possible that the head-to-car body contact may not occur.

These vehicles can cause more severe injuries because of the greater height at the front edge of the hood. In this case pedestrians, especially small pedestrians, are hit in the pelvis–abdomen area with the front end, as opposed to compact class cars where the pelvis and abdomen were hit by the hood.

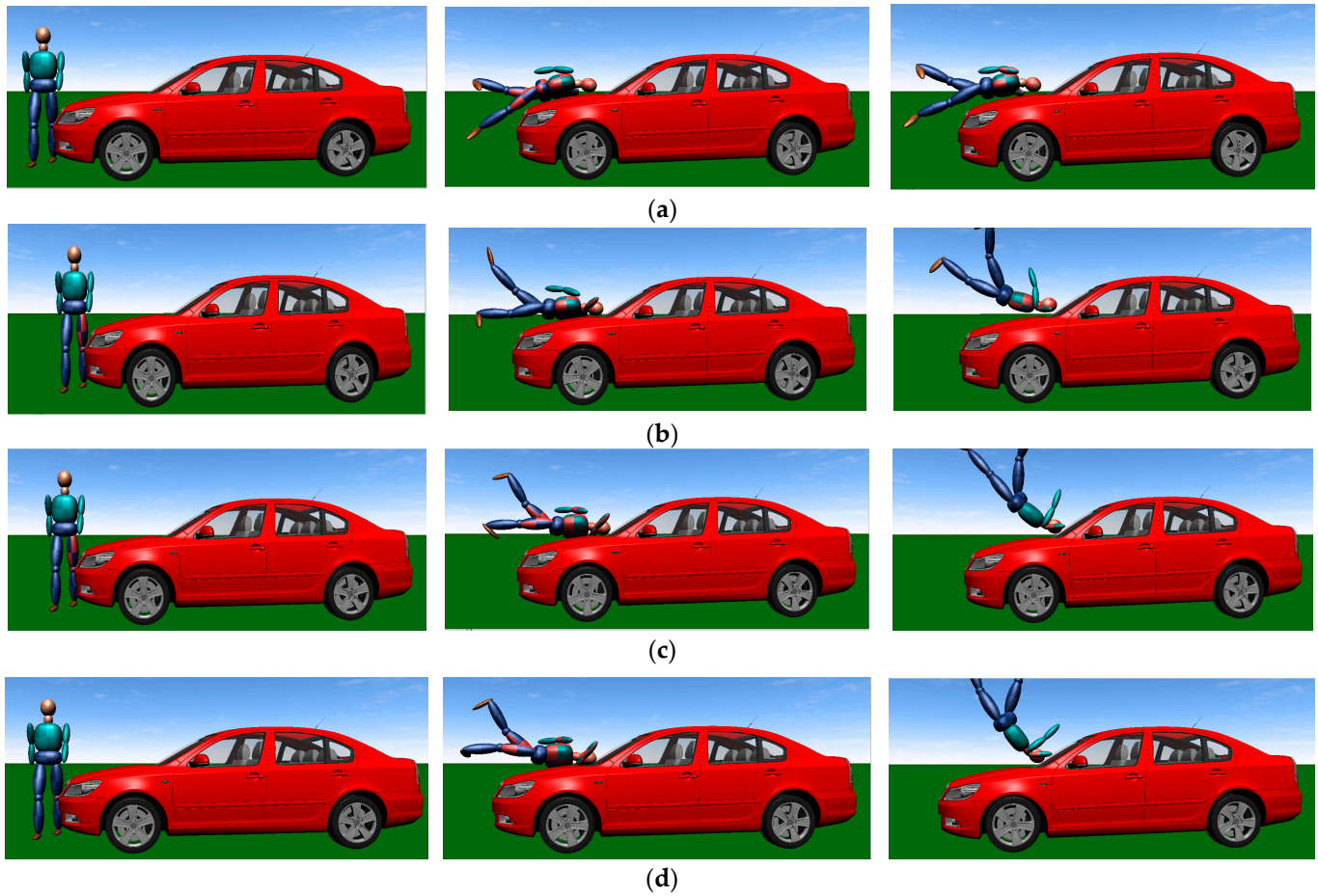

Figure 7. Example of collision, compact class vehicle, at (**a**) 5 m/s, (**b**) 10 m/s, (**c**) 15 m/s and (**d**) 20 m/s, with deceleration of 2.5 m/s^2.

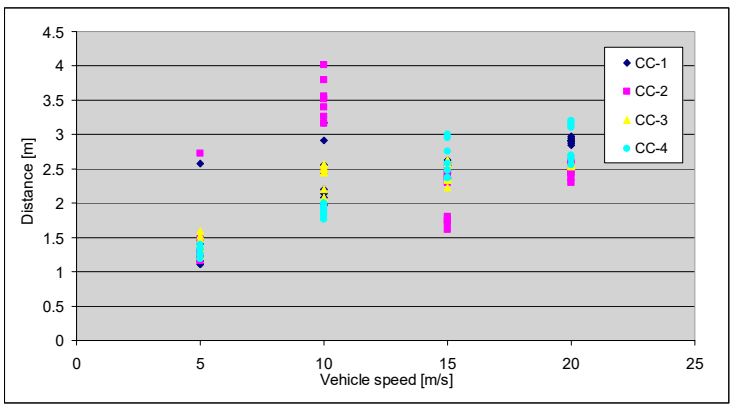

Figure 8. Carry distance for compact class vehicle.

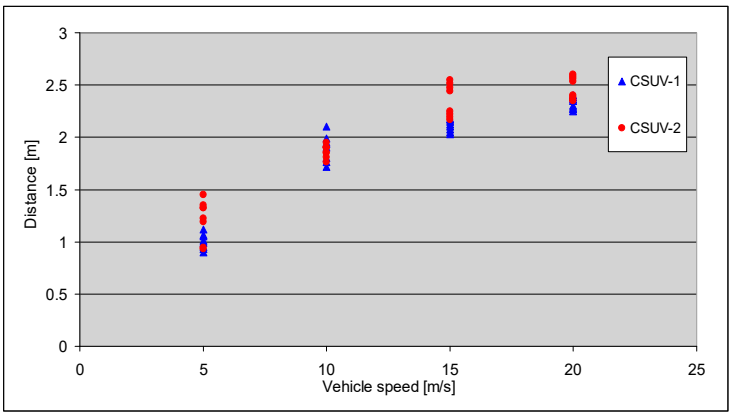

Figure 9. Carry distance for CSUV class vehicle.

Figure 10. Example of collision for CSUV vehicle, at 5 m/s speed.

The results by type of vehicle show, as indicated in Figure 11, the longest distances travelled by the pedestrian in contact with the car, until detachment from the car for the SM class. The maximum distance in this case is just over 4.3 m at 10 m/s, as seen in Figure 12. In this case, for 10 m/s speed, there is a great dispersion, as a function of impact speed, of the distances travelled during the contact phase. The minimum distance is 1.15 m at a collision speed of 5 m/s. For this class of cars, at low impact speeds, the pedestrian kinematics is wrap around, followed by the somersault and roof vault at 20 m/s.

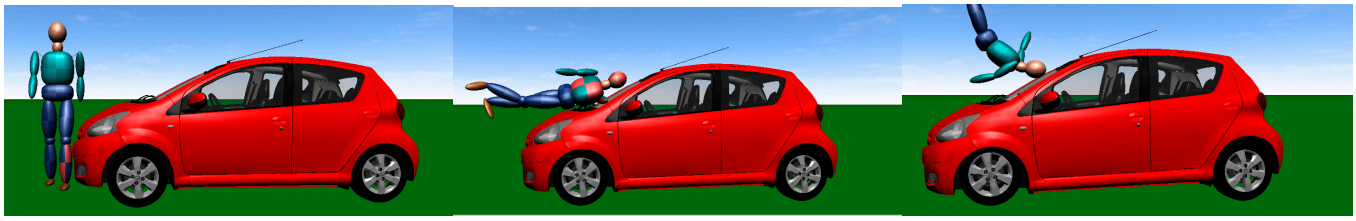

Figure 11. Impact phases for SM class vehicle.

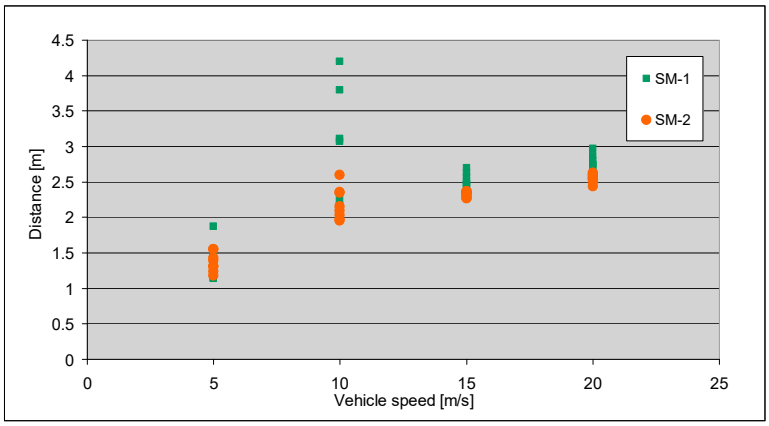

Figure 12. Carry distance for SM class vehicle.

Considering the time origin at the moment of impact between the bumper and the pedestrian's lower limb, the secondary collision occurs within the time range of 0.05 s to 0.245 s, and the detachment from the car within the time range of 0.125 s to 0.42 s.

For executive class EC, as indicated in Figure 13, the maximum distance in this case is around 2.5 m at 20 m/s, as displayed in Figure 14. The minimum distance is 1.2 m at a collision speed of 5 m/s. For this class of cars, at low impact speeds, the pedestrian kinematics is wrap around, followed by the somersault after 10 m/s.

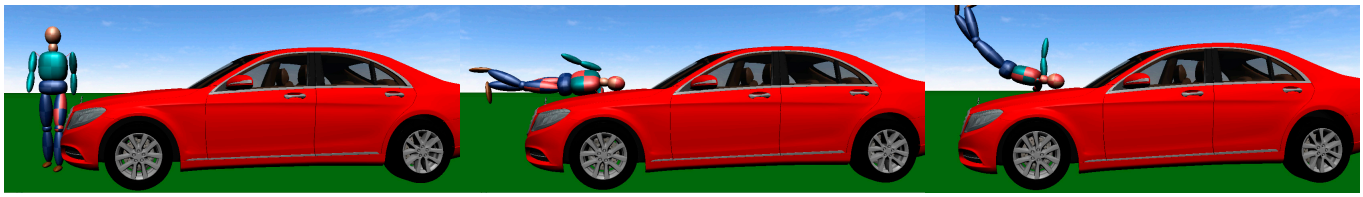

Figure 13. Impact phases for executive class vehicle.

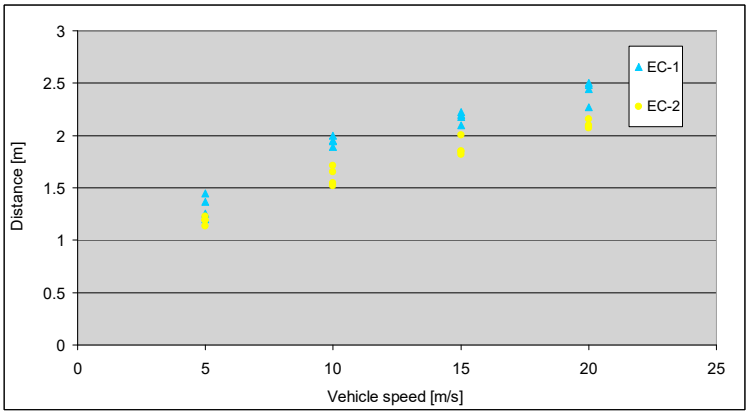

Figure 14. Carry distance for executive class vehicle.

Considering the time origin at the moment of impact between the bumper and the pedestrian's foot, the secondary collision occurs within the time range of 0.06 s to 0.24 s, and the detachment from the car within the time range of 0.105 s to 0.315 s.

For all classes of vehicles, we observe a tendency to increase the distance covered during the contact phase, along with the increase in the impact speed. The posture of the pedestrian at the moment of impact generates the kinematics of his/her movement, but it does not significantly change the contact times or, implicitly, the distances covered, as seen in Figure 15.

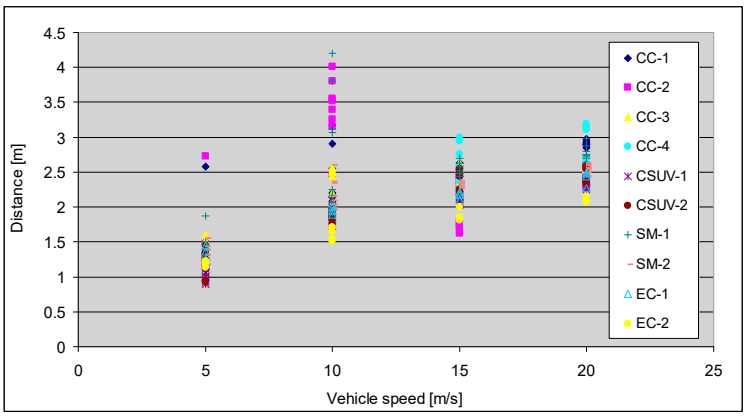

Figure 15. Pedestrian carrying distance for all class vehicles.

Analyzing all the categories of vehicles subjected to simulations as a whole, we notice that as the deceleration increases at the moment of impact, the maximum values of the distance traveled by the pedestrian until the separation from the vehicle decrease, as seen in Figure 16.

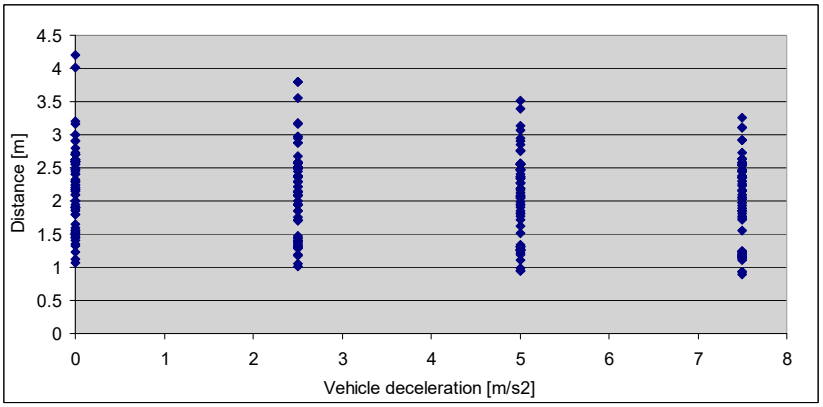

Figure 16. Pedestrian carrying distance as a function of braking deceleration.

For rainy conditions, the adhesion coefficient of the wheels has been changed to the value of 0.4, so the vehicle can brake with a maximum of 3.93 m/s^2. The simulations were run this way only for deceleration of 2.5 m/s^2, varying the impact speed. The coefficient of friction between the car and the pedestrian was reduced to 0.1, whereas the coefficient of friction between the pedestrian and the ground was reduced to 0.3.

Following the simulations, the analysis of the contact force diagrams that appear on the main body segments of the dummy indicates that the detachment times from the passenger car resulted with a maximum variation of 9.38% for all the classes of vehicles studied. Expressed in distance covered, these variations have a mean with a maximum of 0.4 m. The simulations in wet weather show an increase in the separation times compared to those performed for dry asphalt. Examples of these diagrams are shown in Figures 16–20.

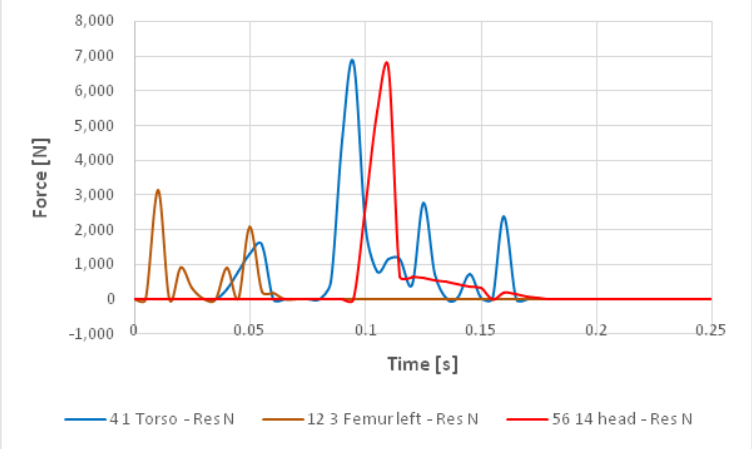

Figure 17. Example of detachment time for SM class at 15 m/s and 2.5 m/s^2 on wet road.

As far as the mass of pedestrians is concerned, simulations were run with pedestrians of 55, 75 and 110 kg, all with the same height. The results of the simulations show a maximum variation of 10% in the time at which the pedestrian detaches from the vehicle, as indicated in Figures 21–26. Pedestrians with a smaller mass detach after a shorter time compared to a 75 kg pedestrian. Pedestrians with a larger mass detach after a longer time, compared to a 75 kg pedestrian. Regarding their kinematics, it can be seen that pedestrians with a large mass have the largest movement, as indicated in Figures 27 and 28.

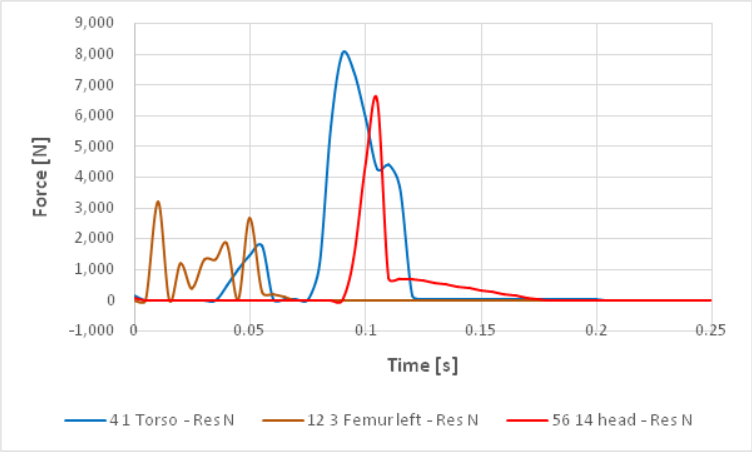

Figure 18. Example of detachment time for SM class at 15 m/s and 2.5 m/s^2 on dry road.

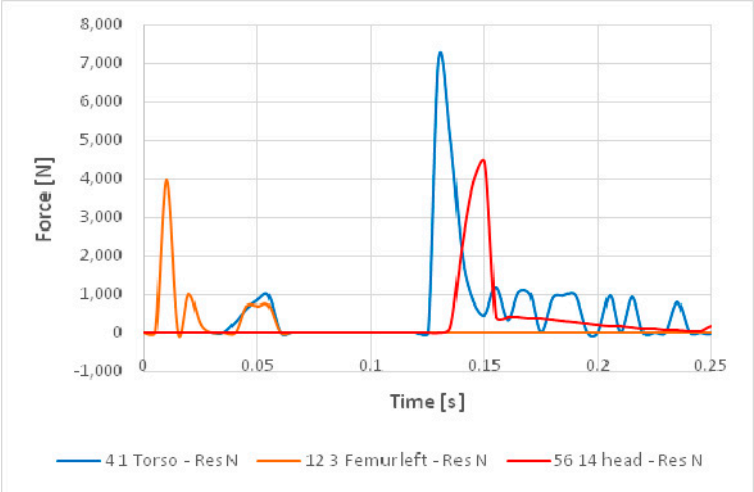

Figure 19. Example of detachment time for CC class at 10 m/s and 2.5 m/s^2 on wet road.

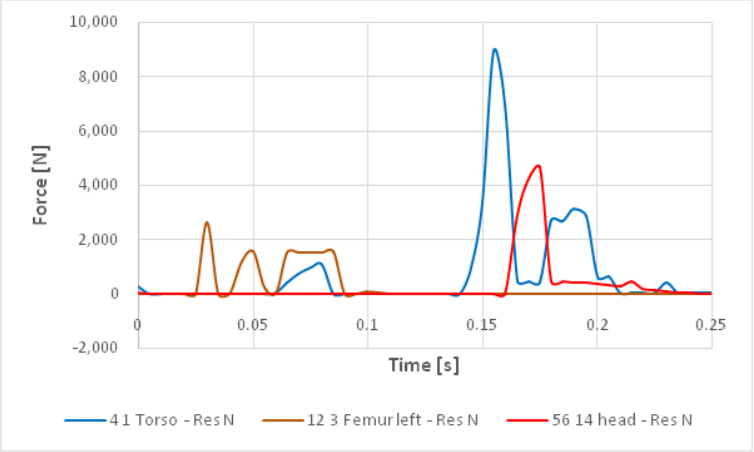

Figure 20. Example of detachment time for CC class at 10 m/s and 2.5 m/s^2 on dry road.

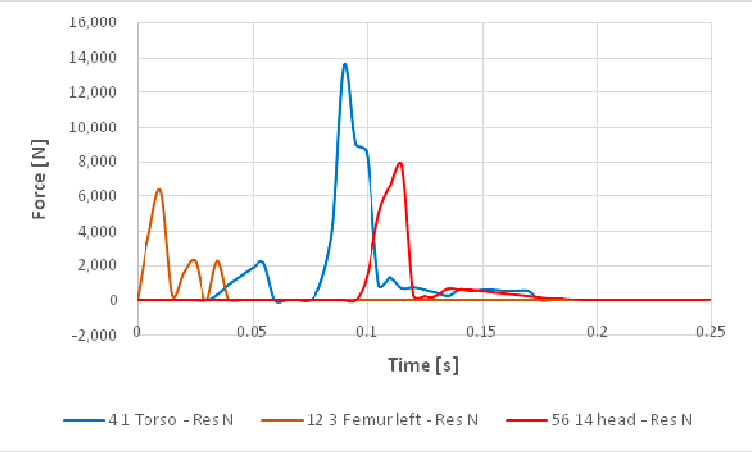

Figure 21. CC at speed of 15 m/s, 5 m/s^2 deceleration and pedestrian mass 110 kg.

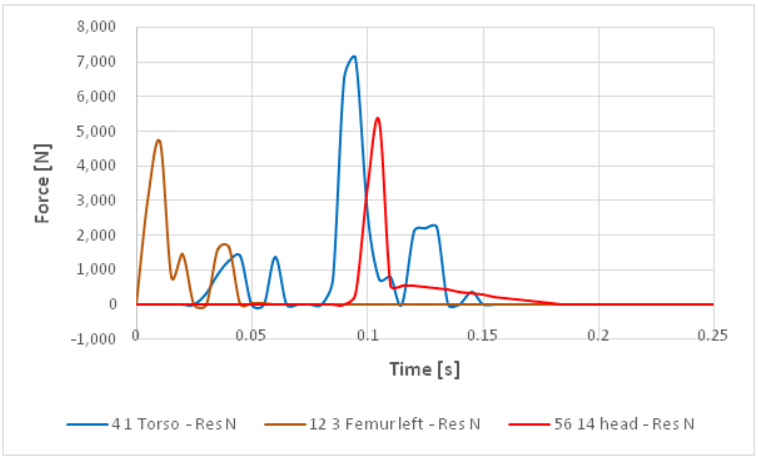

Figure 22. CC at speed of 15 m/s, 5 m/s^2 deceleration and pedestrian mass 55 kg.

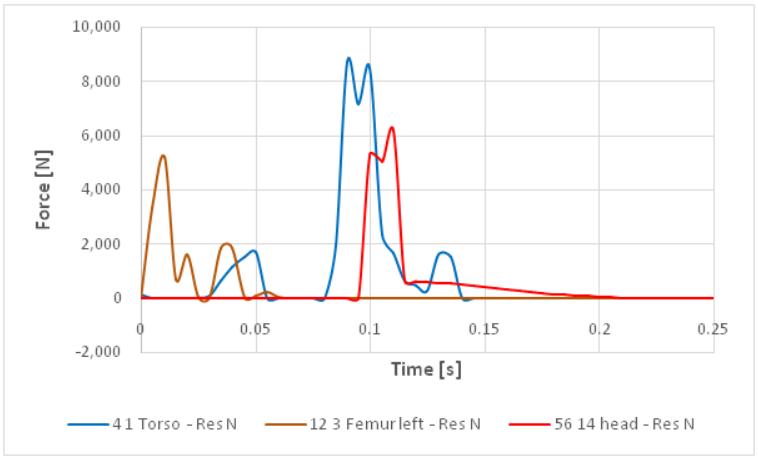

Figure 23. CC at speed of 15 m/s, 5 m/s^2 deceleration and pedestrian mass 75 kg.

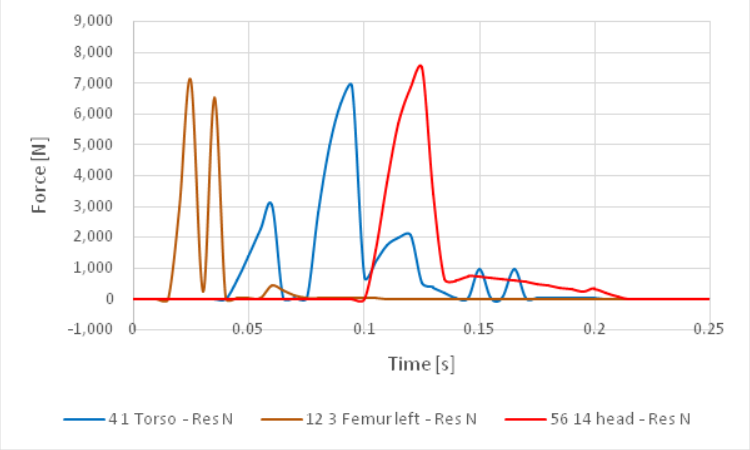

Figure 24. CSUV at speed of 15 m/s, 5 m/s^2 deceleration and pedestrian mass 110 kg.

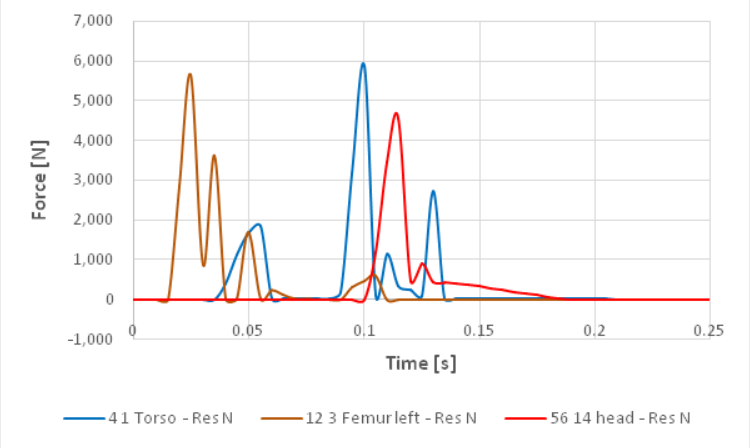

Figure 25. CSUV at speed of 15 m/s, 5 m/s^2 deceleration and pedestrian mass 55 kg.

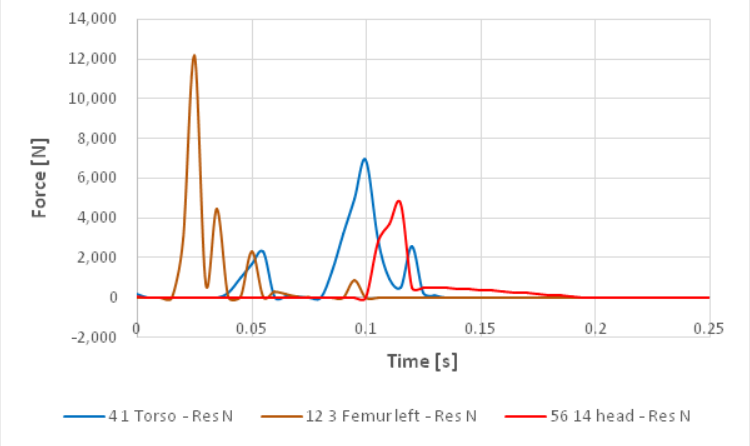

Figure 26. CSUV at speed of 15 m/s, 5 m/s^2 deceleration and pedestrian mass 75 kg.

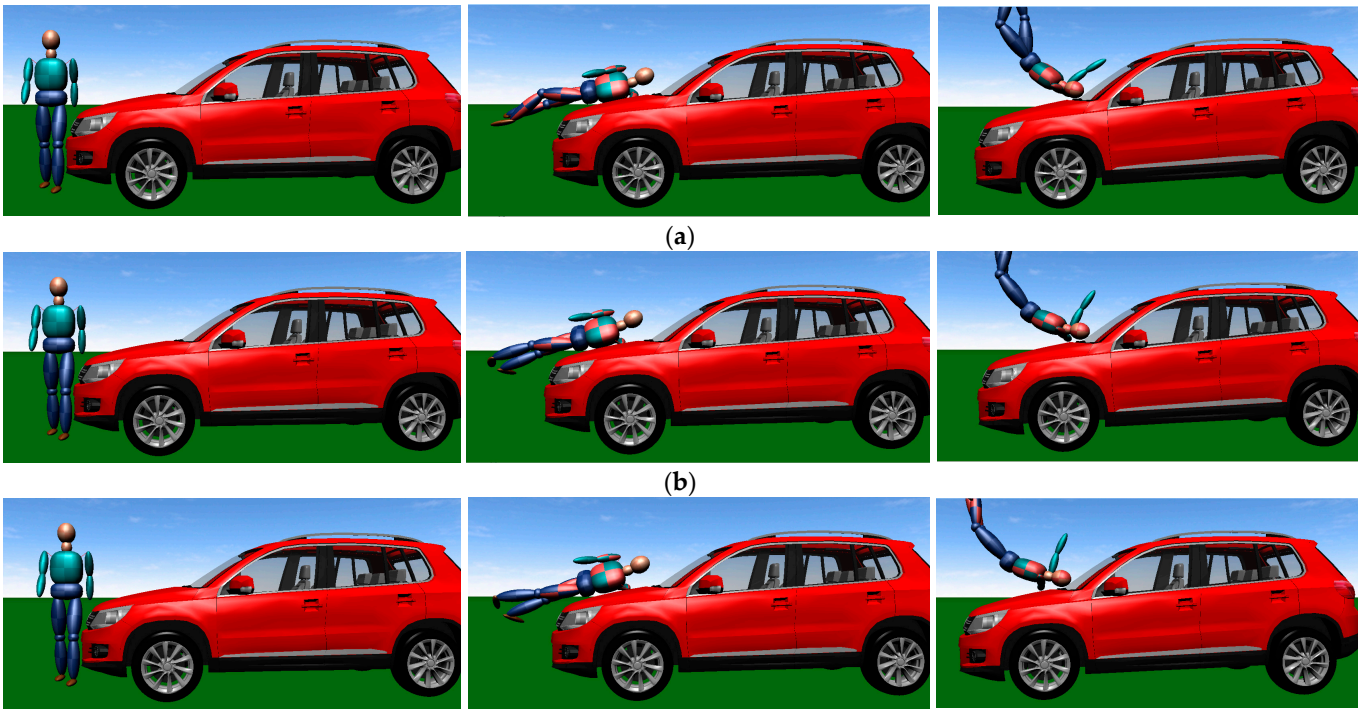

(**a**)

(**b**)

(**c**)

Figure 27. Example of CSUV at speed 15 m/s, deceleration 5 m/s^2, pedestrian mass (**a**) 110 kg, (**b**) 75 kg, (**c**) 55 kg.

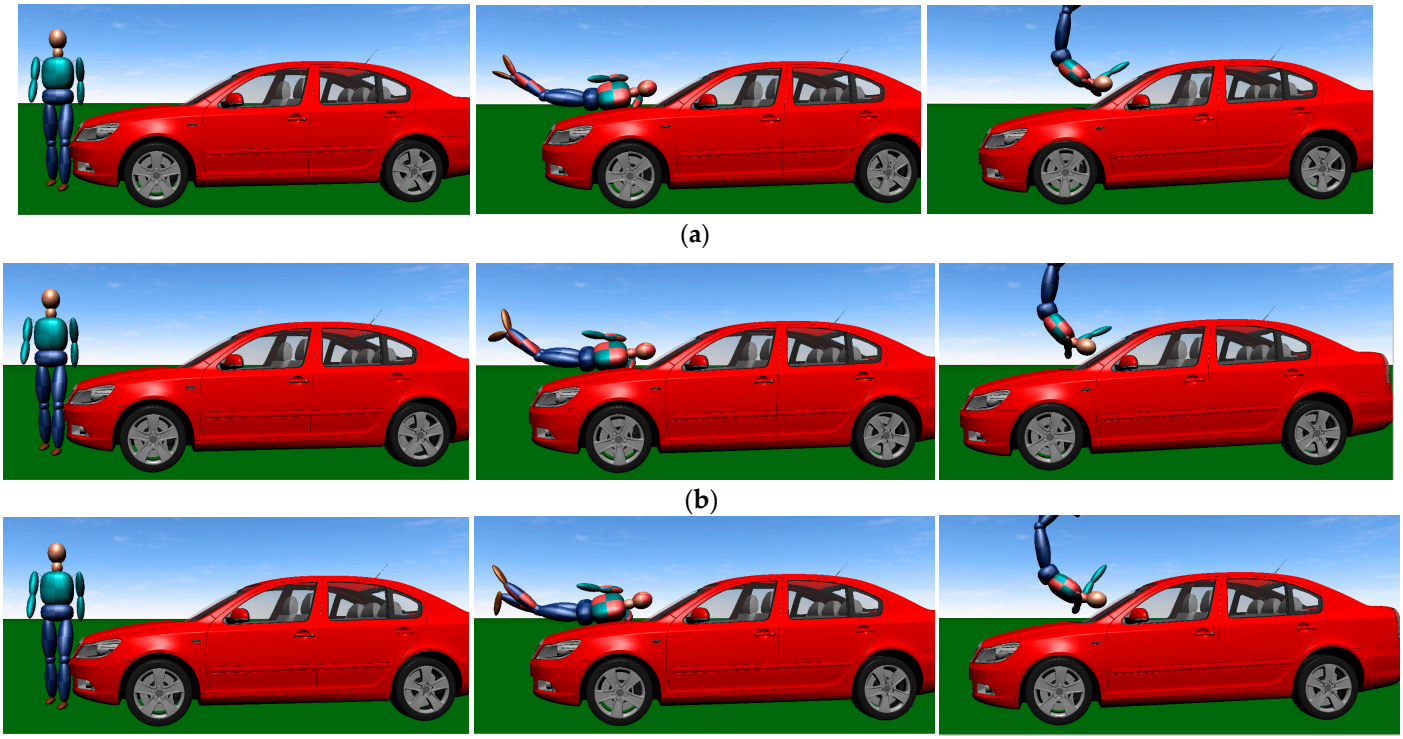

(**a**)

(**b**)

(**c**)

Figure 28. Example of CC at speed 15 m/s, deceleration 5 m/s^2, pedestrian mass (**a**) 110 kg, (**b**) 75 kg, (**c**) 55 kg.

5. Discussion

The current geometry of cars influences the distances traveled by pedestrians coming into contact with them. In the speed range of 10 m/s to 5 m/s, a large dispersion of the values obtained for the distances traveled by the vehicle in contact with the pedestrian can be observed, both in the case of simulations and in the experimental tests. For low speeds, the possible explanation is the fact that the movement of the pedestrian is not extensive; after the impact in the area of the lower limbs, he/she flips over on the hood and remains in contact until he/she slides in front or on the side of the vehicle.

In the simulations that we carried out, the dispersion according to the vehicle class is presented in Table 4. It can be observed that the distance covered during the contact phase between the vehicle and the pedestrians depends on the vehicle class. Thus, SM and CC class vehicles have the longest contact phase distance, followed by CSUV and EC class.

Table 4. Contact distance according to different classes of vehicle.

Vehicle Class	D_{veh}Min	D_{veh}Max	Ratio Dmax/Dmin
CC	1.11	4.01	3.61
CSUV	0.89	2.6	2.92
EC	1.20	2.5	2.08
SM	1.13	4.2	3.71

The experimental research, amounting to 18 tests, were carried out with different types of vehicles, at various impact speeds, with dummies of different sizes and masses or real accidents, as shown in Figure 29a,b. The video images captured during the experiments were analyzed with the aim of establishing the distances traveled by pedestrians in contact with vehicles. They best reproduce the different specific conditions under which accidents involving pedestrians take place. Also, the impact conditions, dry or wet road, varied. An important mention is that the dummies used had various masses and heights, thus covering as large a segment as possible of the anthropometric typologies of people.

(**a**)

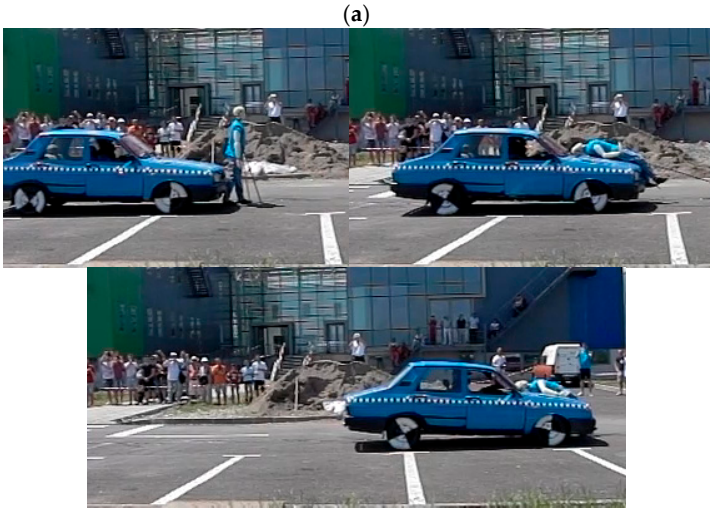

(**b**)

Figure 29. Examples of impact with dummies (**a**,**b**). (**a**) Source [40].

The experimental data confirm the existence of the two sub-phases of the contact between the car and the pedestrian. Superimposing the distances travelled by pedestrians over the simulation results, as displayed in Figure 30, shows a good correlation between them. The large dispersion of the travel distances around the speed of 10 m/s is also evident in the experimental investigations.

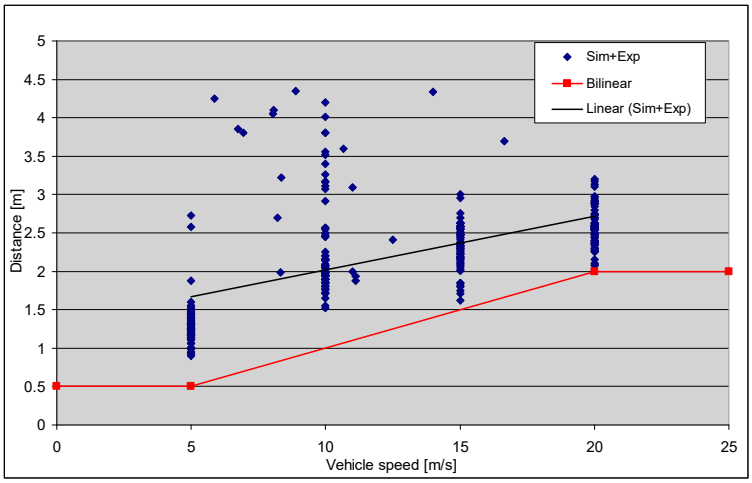

Figure 30. Comparison between carry distance from simulation, experimental tests and bilinear model.

The comparison between the bilinear model and the theoretical and experimental results changes some aspects of the distance travelled during the contact phase between the cars and the pedestrians. Thus, the reconstruction of traffic accidents can be conducted on the basis of new assumptions. A trendline was identified in order to express the difference between these two models, as seen in Figure 30.

Future research could develop a new mathematical model of the pedestrian's distance in contact with the car, taking into consideration more factors such as height of pedestrian, different weather conditions dry/wet/icy, different mass and posture of pedestrian during impact.

The theoretical simulations were run with four classes of vehicles, with their frontal profile influencing the results obtained. The impact speed directly proportionally influences the distance traveled by the vehicle in contact with the pedestrian and inversely proportionally influences the contact times between them.

In the range of speeds 5–10 m/s, the results regarding the distance traveled during the contact phase show the greatest dispersion, both in theoretical simulations and in experimental tests.

Low vehicles, such as coupes, hatchbacks or sedans, at high speeds tend to throw the pedestrian on top of them, while SUVs tend to run over the pedestrian at low speeds, having a fairly high ground clearance; therefore, the contact varies depending on the shape of the vehicle.

Child pedestrians, especially those under the age of 10 and short-heighted, are thrown in front of the vehicle at the time of the collision. For this case, there is no transportation phase by the vehicle, with the impact being of the forward projection type.

6. Conclusions

The studies carried out in the field of car–pedestrian accident analysis have highlighted the existence of three phases in the development of the impact. In more recent studies, the first phase, of contact with the car, was divided into two stages as follows: the contact until the pedestrian hits the vehicle with his/her head or thorax, and the contact until he/she is detached from the vehicle. In the current literature, the distance traveled by the car in contact with the pedestrian was approximated using the bilinear law proposed in [10].

The experimental results and the simulations carried out in the current study have improved the prediction model of the distance traveled by the car during the contact phase with the pedestrian.

The results of the research show that the throwing distance of the pedestrian does not change, but the three distances traveled during the phase of contact with the vehicle, flight and contact with the ground are different, as compared to the previous, which the bilinear model took into account.

The mass of pedestrians, as well as the conditions in which accidents occur (dry/wet), have a maximum influence of 10% on the distance traveled by the pedestrian in contact with the vehicle.

A trendline was obtained, which clearly shows the difference between the current results and the bilinear model.

Author Contributions: Conceptualization, A.S. and B.B.; methodology, A.S. and B.B.; software, A.S. and B.B.; validation, A.S. and B.B.; formal analysis, A.S. and B.B.; investigation, A.S. and B.B.; resources, A.S. and B.B.; data curation, A.S. and B.B.; writing—original draft preparation, A.S. and B.B.; writing—review and editing, A.S. and B.B.; visualization, A.S. and B.B.; supervision, A.S.; project administration, A.S. All authors have read and agreed to the published version of the manuscript.

Funding: This research received no external funding.

Data Availability Statement: Not applicable.

Conflicts of Interest: The authors declare no conflict of interest.

References

1. Collins, J.C.; Moris, J.L. *Highway Collision Analysis*; Thomas Publishing: New York, NY, USA, 1979.
2. Wood, D.; Simms, C. Coefficient of Friction in Pedestrian Throw. *Impact J. ITAI* **2000**, *9*, 12–14.
3. Searle, J.A. *The Physics of Throw Distance in Accident Reconstruction*; SAE Technical Paper Series; SAE International: Warrendale, PA, USA, 1993; p. 930659.
4. Searle, J.A.; Searle, A. The Trajectories of Pedestrians, Motorcycles, Motorcyclists, etc., Following a Road Accident. SAE Technical Paper Series. In Proceedings of the 27th Stapp Car Crash Conference with IRCOBI and Child Injury and Restraint Conference with IRCOBI, San Diego, CA, USA, 17–19 October 1983; p. 831622.
5. Kuhnel, A. Der FahrzeugFussgangerUnfall und Seine Rekonstruktion. Ph.D. Thesis, TU-Berlin, Berlin, Germany, 1980.
6. Eubanks, J.J.; Haight, W.R. *Pedestrian Involved Traffic Collision Reconstruction Methodology*; SAE Technical Paper Series; SAE International: Warrendale, PA, USA, 1992; Volume 101-6, p. 921591.
7. Limpert, R. *Motor Vehicle Accident Reconstruction and Cause Analysis*, 5th ed.; Lexis Publishing: Charlottesville, WV, USA, 1999; pp. 539–554.
8. Ravani, B.; Brougham, D.; Masson, R.T. Pedestrian Post Impact Kinematics and Injury Pattern; SAE Technical Paper Series. In Proceedings of the 25th Stapp Car Crash Conference, San Francisco, CA, USA, 28–30 September 1981; p. 811024.
9. Brooks, D.; Wiechel, J.; Sens, M.; Guenther, D. *A Comprehensive Review of Pedestrian Impact Reconstruction*; SAE Technical Paper Series; SAE International: Warrendale, PA, USA, 1987; Volume 96, p. 890859.
10. Han, I.; Brach, R.M. Throw Model for Frontal Pedestrian Collisions; SAE Technical Paper Series. In Proceedings of the SAE 2001 World Congress, Detroit, Michigan, 5–8 March 2001.
11. Batista, M. A Simple Throw Model For Frontal Vehicle Pedestrian Collisions. *Promet-Traffic Transp.* **2008**, *20*, 357–368.
12. Soica, A.; Tarulescu, S. Impact Phase in Frontal Vehicle-Pedestrian Collisions. *Int. J. Automot. Technol.* **2016**, *17*, 387–397. [CrossRef]
13. Shang, S.; Teeling, D.; Masson, C.; Arnoux, P.-J.; Py, M.; Ferrand, Q.; Simms, C.K. Pedestrian Head Injuries in Ground Contact: A Cadaver Study. In Proceedings of the IRCOBI Conference, Florence, Italy, 11–13 September 2019.
14. Ahlgrimm, J.; Burg, H.; Dettinger, J.; Dettinger, J.; Moser, A. Fußgängerunfälle. In *Handbuch Verkehrsunfallrekonstruktion*; Burg, H., Moser, A., Eds.; Springer: Vieweg Wiesbaden, Germany, 2017; Chapter A10; pp. 391–426.
15. Moser, A.; Hoschopf, H.; Steffan, H.; Kasanicky, G. Validation of the PC-Crash Pedestrian Model. *SAE Trans.* **2000**, *109*, 1316–1339.
16. Fatzinger, E.; Landerville, J.; Tovar, J.; Nguyen, B. Validation of a PC-Crash Multibody Sport Bike Motorcycle Model. *SAE Int. J. Adv. Curr. Prac. Mobil.* **2021**, *3*, 1682–1914. [CrossRef]
17. Páez, F.-M.; Furones, A.; Sánchez, S. Pedestrian-Vehicle Accidents Reconstruction with PC-Crash®: Sensibility Analysis of Factors Variation. In Proceedings of the XII Conference on Transport Engineering, CIT 2016, Valencia, Spain, 7–9 June 2016; Transportation Research Procedia, 18; pp. 115–121.
18. Lobo, A.; Ferreira, S.; Iglesias, I.; Couto, A. Daily and Latent Lagged Effects of Rainfall on Pedestrian–Vehicle Collisions. *Weather Clim. Soc.* **2019**, *12*, 279–291. [CrossRef]

19. Yannis, G.; Karlaftis, M.G. Weather Effects on Daily Traffic Accidents and Fatalities: A Time Series Count Data Approach. In Proceedings of the Conference: Transportation Research Board 89th Annual Meeting, Washington, DC, USA, 10–14 January 2010.
20. Staines, T. Car Crashes and the Weather: An Exploratory Analysis of Environmental Conditions' Impact on Traffic Accident Rates. *Towards Data Sci.* **2018**. Available online: https://towardsdatascience.com/car-crashes-and-the-weather-an-exploratory-analysis-of-environmental-conditions-impact-on-traffic-12bcb7f9afed (accessed on 7 July 2023).
21. Wdowicz, D.; Ptak, M. Numerical Approaches to Pedestrian Impact Simulation with Human Body Models: A Review. *Arch. Comput. Methods Eng.* **2023**. [CrossRef]
22. PC-CRASH. *A Simulation Program for Vehicle Accidents, Operating and Technical Manual*; Version 13.1; Dr. Steffan Datentechnik: Linz, Austria, 21 July 2021.
23. Spit, H.H. *Evaluation of PC Crash: As Tool for Professional Traffic Accident Research and Reconstruction*; DCT Rapporten; Technische Universiteit Eindhoven: Eindhoven, The Netherlands, 2000.
24. Dongjun, K.; Jaehoon, S. Analysis of Pedestrian Accidents Based on In-vehicle Real Accident Videos. In Proceedings of the 23rd International Technical Conference on the Enhanced Safety of Vehicles (ESV), Seoul, Republic of Korea, 27–30 May 2013.
25. Han, Y.; Li, Q.; Wang, F.; Wang, B.; Mizuno, K.; Zhou, Q. Analysis of pedestrian kinematics and ground impact in traffic accidents using video records. *Int. J. Crashworthiness* **2019**, *24*, 211–220. [CrossRef]
26. Matsui, Y.; Takahashi, K.; Imaizumi, R.; Ando, K. Car-To-Pedestrian Contact Situations In Near-Miss Incidents And Real-World Accidents In Japan. *Traffic Inj. Prev.* **2013**, *14*, 58–63. [CrossRef] [PubMed]
27. Untaroiu, C.D.; Meissner, M.U.; Crandall, J.R.; Takahashi, Y.; Okamoto, M.; Ito, O. Crash reconstruction of pedestrian accidents using optimization techniques. *Int. J. Impact Eng.* **2009**, *36*, 210–219. [CrossRef]
28. Crocetta, G.; Piantini, S.; Pierini, M.; Simms, C. The influence of vehicle front-end design on pedestrian ground impact. *Accid. Anal. Prev.* **2015**, *79*, 56–69. [CrossRef] [PubMed]
29. Shang, S.; Masson, C.; Llari, M.; Py, M.; Ferrand, Q.; Arnoux, P.-J.; Simms, C. The predictive capacity of the MADYMO ellipsoid pedestrian model for pedestrian ground contact kinematics and injury evaluation. *Accid. Anal. Prev.* **2021**, *149*, 105803. [CrossRef] [PubMed]
30. Posirisuk, P.; Baker, C.; Ghajari, M. Computational prediction of head-ground impact kinematics in e-scooter falls. *Accid. Anal. Prev.* **2022**, *167*, 106567. [CrossRef] [PubMed]
31. Van Rooij, L.; Bhalla, K.; Meissner, M.; Ivarsson, J.; Crandall, J.; Longhitano, D.; Takahashi, Y.; Dokko, Y.; Kikuchi, Y. Pedestrian crash reconstruction using multi-body modeling with geometrically detailed, validated vehicle models and advanced pedestrian injury criteria. In Proceedings of the 18th International Technical Conference on the Enhanced Safety of Vehicles (ESV), Nagoya, Japan, 19–22 May 2003.
32. Deng, G.; Wang, F.; Yu, C.; Peng, Y.; Xu, H.; Li, Z.; Hou, L.; Wang, Z. Assessment of standing passenger traumatic brain injury caused by ground impact in subway collisions. *Accid. Anal. Prev.* **2022**, *166*, 106547. [CrossRef] [PubMed]
33. Liu, Y.; Wan, X.; Xu, W.; Shi, L.; Deng, G.; Bai, Z. An intelligent method for accident reconstruction involving car and e-bike coupling automatic simulation and multi-objective optimizations. *Accid. Anal. Prev.* **2022**, *164*, 106476. [CrossRef] [PubMed]
34. Stevenson, T.J. Simulation Of Vehicle-Pedestrian Interaction. Ph.D. Thesis, University of Canterbury, Christchurch, New Zealand, 2006.
35. Xiaoyun, Z.; Xinyi, H.; Dongming, Z.; Xiaobo, Y. Research of non-linear frictional contact model in vehicle-pedestrian accidents based on computer simulation. *Int. J. Crashworthiness* **2020**, *25*, 351–359. [CrossRef]
36. Zou, D.; Fan, Y.; Liu, N.; Zhang, J.; Liu, D.; Liu, Q.; Li, Z.; Wang, J.; Huang, J. Multiobjective optimization algorithm for accurate MADYMO reconstruction of vehicle-pedestrian accidents. *Front. Bioeng. Biotechnol.* **2022**, *10*, 1032621. [CrossRef] [PubMed]
37. Savelberg, H.; Meijer, K. The Effect of Age and Joint Angle on the Proportionality of Extensor and Flexor Strength at the Knee Joint. *J. Gerontology. Ser. A Biol. Sci. Med. Sci.* **2004**, *59*, 1120–1128. [CrossRef] [PubMed]
38. Mooney, L.; Herr, H. Biomechanical walking mechanisms underlying the metabolic reduction caused by an autonomous exoskeleton. *J. NeuroEngineering Rehabil.* **2016**, *13*, 4. [CrossRef] [PubMed]
39. Sentaro, K.; Takanori, I.; Tadamitsu, M.; Toshihiko, H. Three-Dimentional Neck Kinematics during Breakfall ForOsoto-Gari and Its Association with Neck Flexion Strength in Novice Judokas. In Proceedings of the 35th Conference of the International Society of Biomechanics in Sports, Cologne, Germany, 14–18 June 2017.
40. Togănel, G. Cercetări Privind Influenta Designului Caroseriei Asupra Siguranței Pasive a Automobilelor. Ph.D. Thesis, Transilvania University of Brasov, Brasov, Romania, 2008.